DOI: 10.1002/chem.200800159

p-Phenyleneethynylene Molecular Wires: Influence of Structure on Photoinduced Electron-Transfer Properties

Mateusz Wielopolski,[a] Carmen Atienza,[a, b] Timothy Clark,[c] Dirk M. Guldi,*[a] and Nazario Martín*[b, d]

Abstract: A series of donor–acceptor arrays (exTTF–oPPE–C_{60}) containing π-conjugated oligo(phenyleneethynylene) wires (oPPE) of different length between π-extended tetrathiafulvalene (exTTF) as electron donor and fullerene (C_{60}) as electron acceptor has been prepared by following a convergent synthesis. The key reaction in these approaches is the bromo–iodo selectivity of the Hagihara–Sonogashira reaction and the deprotecting of acetylenes with different silyl groups to afford the corresponding donor–acceptor conjugates in moderate yields. The electronic interactions between the three electroactive species were determined by using UV-visible spectroscopy and cyclic voltammetry. Our studies clearly confirm that, although the C_{60} units are connected to the exTTF donor through π-conjugated oPPE frameworks, no significant electronic interactions are observed in the ground state. Theoretical calculations predict how a simple exchange from C=C double bonds (i.e., oligo(*p*-phenylenevinylene) to C≡C triple bonds (i.e., oPPE) in the electron donor–acceptor conjugates considerably alters long-range electron transfer. Photoexcitation of exTTF–oPPE–C_{60} leads to the following features: a transient photoproduct with maxima at 660 and 1000 nm, which are unambiguously attributed to the photolytically generated radical-ion-pair state, [exTTF$^{\bullet+}$–oPPE–$C_{60}^{\bullet-}$]. Both charge-separation and charge-recombination processes give rise to a molecular-wire behaviour of the oPPE moiety with an attenuation factor (β) of (0.2 ± 0.05) Å^{-1}.

Keywords: charge transfer · cross-coupling · donor–acceptor systems · fullerenes · phenyleneethynylene

Introduction

One of the major challenges in current chemistry is to find molecules able to move charges rapidly and efficiently from, for example, one terminus to another under the control of an external electrical, electrochemical or photochemical stimulus.

Nature has provided impressive examples of how these goals can be achieved. The photosynthetic reaction centre protein moves electrons with near-unity quantum efficiency across a lipid bilayer membrane rapidly by using several redox cofactors, and thus serves as a model for developing biomimetic analogues for applications in fields such as photovoltaic devices, molecular electronics and photonic materials.[1]

In this context, π-conjugated oligomeric systems are of particular interest because they provide an efficient electronic coupling between electroactive units—donor and acceptor termini—and display wirelike behaviour. Different factors are required to make a molecule able to behave as an ideal molecular wire: 1) matching between the donor (acceptor) and bridge energy levels, 2) good electronic coupling

[a] M. Wielopolski, Dr. C. Atienza, Prof. Dr. D. M. Guldi
Department of Chemistry and Pharmacy
Interdisciplinary Center for Molecular Materials (ICMM)
Friedrich-Alexander-Universität Erlangen-Nürnberg
Egerlandstrasse 3, 91058 Erlangen (Germany)
Fax: (+49) 913-185-28307
E-mail: dirk.guldi@chemie.uni-erlangen.de

[b] Dr. C. Atienza, Prof. Dr. N. Martín
Departamento de Química Orgánica I
Facultad de Ciencias Químicas
Universidad Complutense, 28040 Madrid (Spain)
Fax: (+34) 91-394-4103
E-mail: nazmar@quim.ucm.es

[c] Prof. Dr. T. Clark
Computer-Chemie-Centrum
Interdisciplinary Center for Molecular Materials
Friedrich-Alexander-Universität Erlangen-Nürnberg
Naegelsbachstrasse 25, 91052 Erlangen (Germany)

[d] Prof. Dr. N. Martín
Instituto Madrileño de Estudios Avanzados en Nanociencia
(IMDEA-Nanociencia), 28049 Madrid (Spain)

Supporting information for this article is available on the WWW under http://www.chemeurj.org/ or from the author.

between the electron donor and acceptor units by means of the bridge orbitals[2] and 3) a small attenuation factor (β).[3]

Among the many different π-conjugated oligomers, oligo(*p*-phenylenevinylene) (oPPV)[4] has emerged as a particularly promising model system that helps to comprehend/rationalise the basic features of poly(*p*-phenylenevinylene) and also as a versatile building block for novel materials with chemically tailored properties.[5] In this context, intramolecular electron transfer along conjugated chains of oPPV has been tested in several donor–acceptor conjugates involving anilines,[6] porphyrins[7] or ferrocenes[8] as electron donors on one side, and [60]fullerenes, on the other side, as the electron acceptor.[9] In fact, in a pioneering study tetracene (TET; as electron donor) and pyromellitimide (PYR; as electron acceptor) were connected by means of oPPV of increasing length (TET–oPPV–PYR).[10] This work has demonstrated the importance of energy matching between the donor and bridge components for achieving molecular-wire behaviour. Quantum-chemical calculations showed a competition between a direct superexchange process and a two-step "bridge-mediated" process, whose efficiency depends primarily on the length and nature of the conjugated bridge.[11]

A more recent study reports on a series of *p*-phenylene oligomers (Ph_n) that bridge phenothiazine (PTZ) and perylene-3,4:9,10-bis(carboximide) (PDI) as electron donor and acceptor, respectively.[12] In this case, the relative contributions of both the coherent superexchange and incoherent hopping mechanisms to the overall charge-transport process were quantified. Moreover, it has been shown that when an oligofluorene is used as a bridge, the electronic structure of the oligomer provides means to access the wirelike incoherent hopping regime for hole transport over long distances at nearly constant bridge energy.[2a]

Our own contributions to this intriguing field include the demonstration of molecular wirelike behaviour in a series of oligo(*p*-phenylenevinylene)s (oPPVs) of variable length. The different oPPV bridges were connected to an electron-accepting [60]fullerene and to a π-extended tetrathiafulvalene (exTTF), which serves as an electron donor. From an analysis of different electron-conduction distances up to 40 Å, we obtained exceptionally low attenuation factors (β) of (0.01 ± 0.005) $Å^{-1}$.[13] The general validity of this conclusion was confirmed by testing metalloporphryins instead of exTTF as electron donors.[14]

Encouraged by these results, we now describe a series of novel donor–acceptor conjugates (exTTF–oPPE–C_{60}) implementing oligo(*p*-phenyleneethynylene) (oPPE) as a bridge.[15] We have started with selective palladium-catalysed cross-coupling reactions of terminal alkynes with aryl halides to increase the length of the molecular wire systematically.[16] Electrochemical studies using cyclic voltammetry and the determination of the photophysical properties by means of fluorescence and transient absorption spectroscopies complement the synthetic work.

Results and Discussion

Synthesis: The synthesis of exTTF–oPPE–C_{60} is based on the preparation of π-conjugated oligo(*p*-phenyleneethynylene) building blocks using the palladium-catalysed cross-coupling reaction of terminal alkynes with aryl halides. This protocol provides an efficient and versatile means of extending π conjugation in organic compounds.[16]

The oligo(*p*-phenyleneethynylene) precursors (**6**, **14** and **24**) were asymmetrically functionalised with terminal formyl and alkyne groups, which are, in turn, required for connecting the two electroactive units (exTTF and C_{60}).

The key steps in the synthesis of the oligomeric spacer are the selective palladium-catalysed coupling of terminal alkynes[17] with aryl iodides in the presence of aryl bromides,[18] and the selective removal of the trimethylsilyl (TMS) protecting groups in the presence of triisopropylsilyl (TIPS) groups. Thus, the synthesis of building block **14** was carried out analogously to a literature procedure.[19] The initial dihalogenated derivative **4** was prepared from hydroquinone (**1**) with hexylbromide to give 1,4-dihexyloxybenzene (**2**) in a yield of 80%. Bromination and subsequent iodination reactions gave 2-bromo-5-iodo-1,4-dihexyloxybenzene (**4**) in a yield of 66% (Scheme 1).[20] The introduction of the appropriate ethynyl groups at different stages of the synthetic procedure was carried out by means of the Hagihara–Sonogashira reaction.[21] The experimental conditions were optimised for each step to improve the yield of the target molecules and to reduce undesired homocoupling reactions.[22]

From the initial dihalogenated derivative **4** and using palladium and copper iodide as catalysts in piperidine at room temperature, the iodine atom was substituted by *p*-ethynylbenzaldehyde by reacting with **6** to give **7** in a yield of 41%. Compound **6** was previously synthesised from commercially available 4-iodobenzaldehyde (**5**) in one step.[23] Similar conditions were used to remove the bromine atom with trimethylsilylacetylene. However, the target product was not obtained in any case. A different approach was carried out through selective palladium-catalysed coupling of trimethylsilylacetylene with aryl iodide **4** leading to **8** in a yield of 87%. Further reaction of **8** with *p*-ethynylbenzaldehyde (**6**) led to **9** together with the homocoupling product **10** in low yields.[24] Although different experimental conditions were tested to improve the yield, the best results were obtained by employing tetrakis(triphenylphosphane)–palladium as the catalyst and diisopropylamine as the base at reflux in toluene (Tol). Under these conditions, the desired compound **9** was obtained in a yield of 65% (Table 1).[25]

An alternative route was followed for oPPE **14**. Here, a palladium-catalysed coupling reaction from **8** with triisopropylsilylacetylene afforded the asymmetric alkyne **11** in a yield of 86%. Selective removal of the TMS group, followed by a Sonogashira reaction with 4-iodobenzaldehyde (**5**) led to **13** in a yield of 67%. The target product **14** was finally obtained by monodeprotection of either **9** or **13** with K_2CO_3 in THF–MeOH, or tetrabutylammonium fluoride (TBAF), respectively, in quantitative yields.

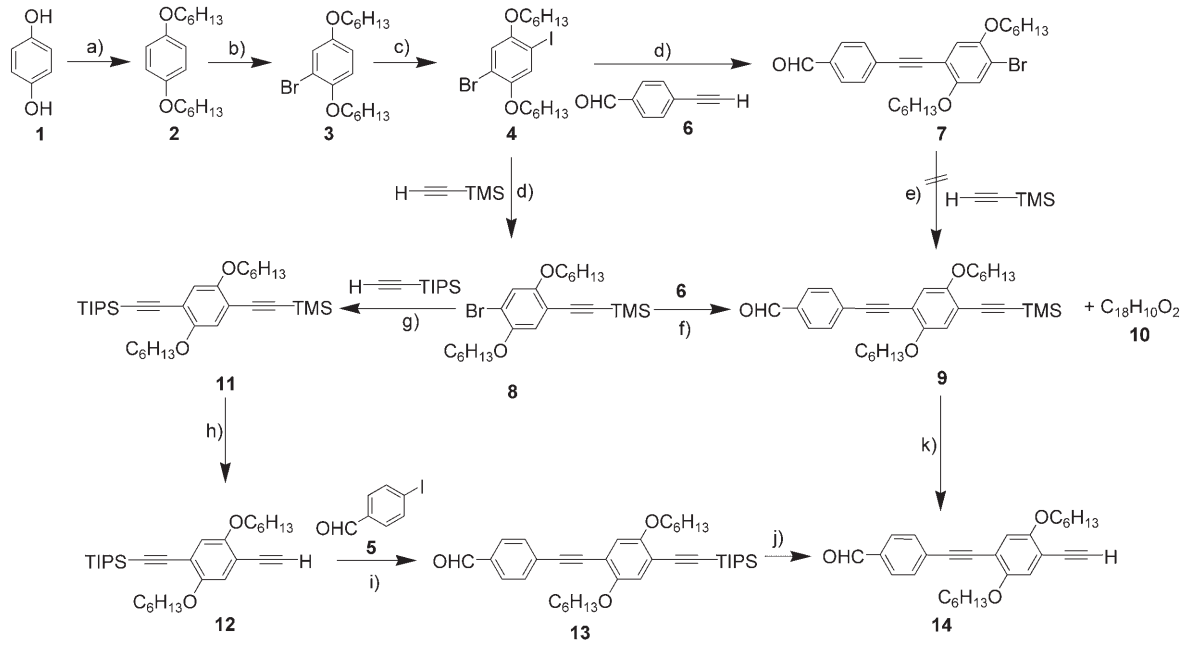

Scheme 1. a) $C_6H_{13}Br$, EtONa, EtOH, Δ, 24 h. b) Br_2, AcONa/AcOH, 0 °C. c) I_2, $H_2SO_4/H_2O/KIO_3$, AcOH/CCl_4/Δ. d) $[PdCl_2(PPh_3)_2]$, PPh_3, CuI, piperidine/RT. e) Different conditions were tested: $[Pd(PPh_3)_4]$, CuI, iPr_2NH, THF/Δ; $Pd(OAc)_2$, PPh_3, EtN_3/Δ; $[PdCl_2(PPh_3)_2]$, CuI, EtN_3, DMF/Δ. f) $[Pd(PPh_3)_4]$, CuI, iPr_2NH, Tol/Δ. g) $[Pd(PPh_3)_4]$, CuI, iPr_2NH, THF/Δ. h) K_2CO_3, THF–MeOH. i) $[Pd(PPh_3)_4]$, CuI, iPr_2NH, THF/Δ. j) Bu_4NF, THF. k) K_2CO_3, THF–MeOH.

Table 1. Experimental conditions used for Sonogashira reactions.

Catalyst	Base	Solvent	*T*	Yield **9**/**10**
$[Pd(PPh_3)_4]$/CuI	iPr_2NH	THF	reflux	10:0
$[Pd(PPh_3)_4]$/CuI	iPr_2NH	THF[a]	reflux	56:5
$[Pd(PPh_3)_4]/AgO_2$	–	THF	reflux	10:0
$[Pd(OAc)_2]/PPh_3$	Et_3N	Et_3N	reflux	3:0
$[Pd(PPh_3)_4]$/CuI	iPr_2NH	toluene	reflux	65:0
$[Pd(dba)_2]$[b]/PPh_3/CuI	iPr_2NEt	toluene	reflux	–
$[PdCl_2(PPh_3)_2]/PPh_3$/CuI	piperidine	piperidine	RT	55:8
$[PdCl_2(PPh_3)_2]/PPh_3$/CuI	iPr_2NH	acetonitrile	RT	45:0

[a] Deoxygenated. [b] dba: dibenzylideneacetone.

The synthesis of the suitably functionalised oPPE **16** was approached through different strategies (Scheme 2). Firstly, the previously synthesised alkynyl **14** was reacted with 2-bromo-5-iodo-1,4-dihexyloxybenzene (**4**) under Sonogashira conditions in the presence of palladium(0)/copper(I) iodide leading to **15** in a yield of 14%. However, the target product **16** could not be obtained by further Sonogashira reactions.

Therefore, we carried out the C–C cross-coupling reactions between **8** and alkynyl compound **14**, from which the homocoupled compound **17** was obtained as the main product. This reaction sequence was studied under different ex-

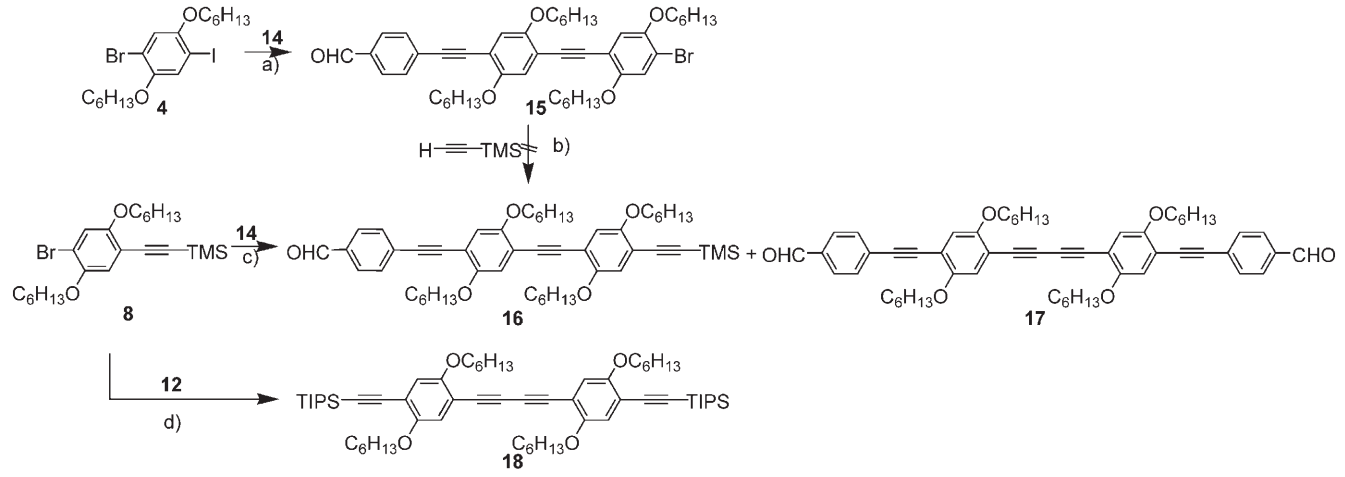

Scheme 2. a) $[Pd(PPh_3)Cl_2]$, PPh_3, CuI, piperidine/RT. b) Different conditions were tested: $[Pd(PPh_3)_4]$, CuI, iPr_2NH, THF/Δ; $Pd(OAc)_2$, PPh_3, EtN_3/Δ. c) $[Pd(PPh_3)_4]$, CuI, iPr_2NH, THF/Δ (Table 2). d) $[Pd(PPh_3)_4]$, CuI, iPr_2NH, THF/Δ.

perimental conditions and, in all cases, the homocoupling compound was obtained as the main product (Table 2).[26]

Table 2. Experimental conditions used for Sonogashira reactions.

Catalyst	Base	Solvent	*T*	Yield **16**/**17**
$[Pd(PPh_3)_4]$/CuI	iPr_2NH	THF	Δ	17:16
$[Pd(PPh_3)_4]$/CuI	iPr_2NH	THF[a]	Δ	8:41
$[Pd(PPh_3)_4]$/CuI	iPr_2NH	toluene	Δ	–
$[PdCl_2(PPh_3)_2]$/CuI	Et_3N	piperidine	RT	0:58
$[PdCl_2(PPh_3)_2]/PPh_3$/CuI	piperidine	piperidine	RT	0:60

[a] Deoxygenated.

Moreover, the Sonogashira reaction between **8** and **12**, in spite of changing the catalyst, base and solvent, afforded exclusively the homocoupling product **18** in a yield of 90%.

We focused on the synthesis of the π-conjugated system **16** by designing an asymmetric ethynyl compound, which allowed selective deprotection of the silyl group and a selective Sonogashira reaction. The incentive was to avoid the undesired homocoupling product (Scheme 3). In this way, selective C–C cross-coupling reactions of terminal alkynyl **12** and aryl iodide **4** and subsequent treatment with trimethylsilylacetylene led to asymmetric compound **20** in a yield of 97%. Selective deprotection of the TMS protecting group and further Sonogashira reaction with 4-iodobenzaldehyde (**5**) afforded compound **16** in a yield of 64%.

This synthetic route led to high yields in all steps and avoided the persistent and undesired homocoupling product. Furthermore, an alternative route was developed based on the halogen interchange to favour the Sonogashira reaction. Thus, treatment of **8** with *n*BuLi and I_2 at room temperature for 12 h afforded **23** in high yields. A further Sonogashira reaction with **14** led to **16** in a yield of 86%. The desired oPPE **24** was obtained by deprotection of **16** and **22** in quantitative yields. The presence of solubilising alkoxy chains lends the oPPEs significant solubility, which allows their full spectroscopic characterisation (Scheme 3).

In the next phase of our synthetic strategy, a palladium-catalysed cross-coupling reaction with copper(I) iodide and triphenylphosphane was carried out to link 2-iodo-π-extended tetrathiafulvalenes (exTTFs) (**25**)[27] to the appropriate spacer oPPEs (**6**, **14**, **24**) in good to moderate yields of 85 (**26a**), 50 (**26b**) and 38% (**26c**) (Scheme 4).

Dyads **26a–c** were fully characterised on the basis of their analytical and spectroscopic data. Importantly, they show in addition to the oPPE features, the presence of exTTF. Thus, the ^{1}H NMR spectra contain singlets at $\delta = 6.30$ (**26a**), 6.95 (**26b**) and 7.04 ppm (**26c**) corresponding to the protons of the 1,3-dithiole rings.

Finally, the target molecules **27a–c** were prepared by 1,3-dipolar cycloadditions of the azomethine ylides, generated in situ from sarcosine (*N*-methylglycine) and aldehydes **26a–c** with C_{60}, as highly soluble brown solids in yields of 33 (**27a**), 63 (**27b**) and 53% (**27c**) (Scheme 5).[28]

A number of spectroscopic techniques were used to determine the structure of exTTF–oPPE–C_{60} (**27a–c**). The FTIR spectra lacked the band at around 1600 cm^{-1}—due to the carbonyl groups—but revealed the presence of the fullerene-specific band at 526 cm^{-1}. The ^{1}H NMR spectra of **27b**, as a representative example, showed, in addition to the aromatic signals, resonance signals of the N–CH_3 group at $\delta =$ 2.86 ppm and the pyrrolidine protons at $\delta = 4.98$ (s, 1H), 5.03 (d, $J = 9.2$ Hz, 1H) and 4.30 ppm (d, $J = 9.2$ Hz, 1H) in good agreement with other *N*-methylfulleropyrrolidine derivatives.[13,14] We also observed the signature of the π-conjugated oPPEs as two singlets at $\delta = 7.03$ and 7.05 ppm and the 1,3-dithiol ring as a singlet at $\delta = 6.79$ ppm (s, 4H).

All of the ^{13}C NMR spectra showed the characteristic signals that correspond to the sp^3 carbon atoms of the pyrroli-

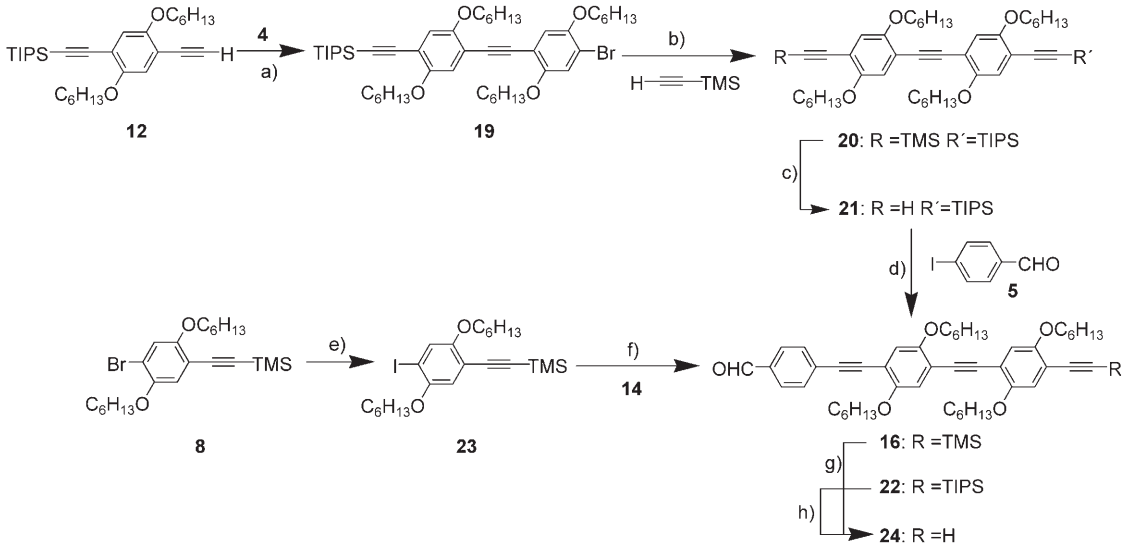

Scheme 3. a) $[Pd(PPh_3)_2Cl_2]$, PPh_3, CuI, piperidine/RT/3 h. b) $[Pd(PPh_3)_4]$, CuI, iPr_2NH, THF/Δ/4 d. c) K_2CO_3, THF–MeOH/RT/2 h. d) $[Pd(PPh_3)_4]$, CuI, iPr_2NH, THF/Δ/28 h. e) *n*BuLi, 0 °C/I_2/RT/12 h. f) $[Pd(PPh_3)_4]$, CuI, iPr_2NH, THF/Δ/28 h. g) K_2CO_3, THF–MeOH/RT/2 h. h) NBu_4F, THF/RT/1 h.

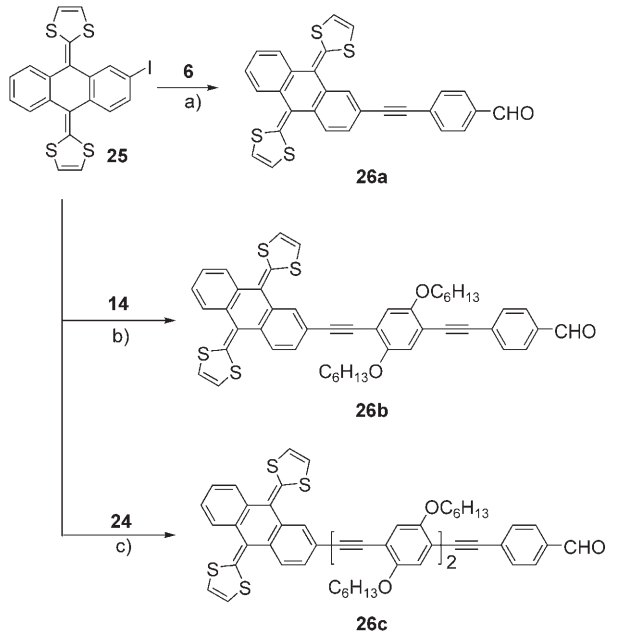

Scheme 4. a) $[PdCl_2(PPh_3)_2]$/CuI/PPh_3/piperidine/RT/24 h. b) $[Pd(PPh_3)_4]$/CuI/iPr_2NH/THF/Δ/3 h. c) $[Pd(PPh_3)_4]$/CuI/iPr_2NH/THF/Δ/48 h.

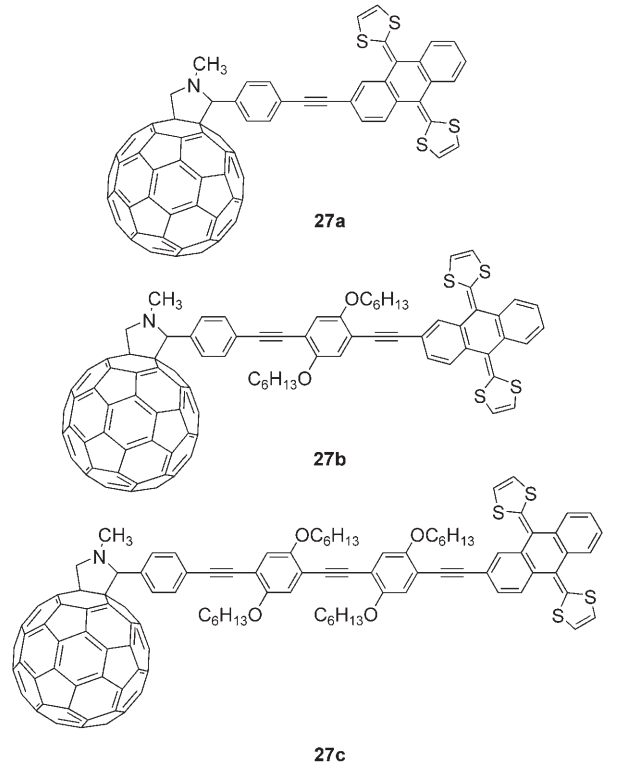

Scheme 5. General conditions for the preparation of triads **27a–c** from (**26a–c**):C_{60} are as follows: *N*-methylglycine, Δ, 3 h in chlorobenzene.

dine ring between $\delta = 70$ and 80 ppm and the tetragonal carbon atoms of the solubilised alkoxy chains (see the Experimental Section in the Supporting Information).

For the electrochemical and photophysical studies, reference compounds **28** and **29** were synthesised as outlined in Scheme 6. Treatment of **9** and **15** with C_{60} and sarcosine (*N*-methylglycine) in chlorobenzene at reflux for 3 h afforded the reference compounds (**28** and **29**) in moderate yields (Scheme 6).

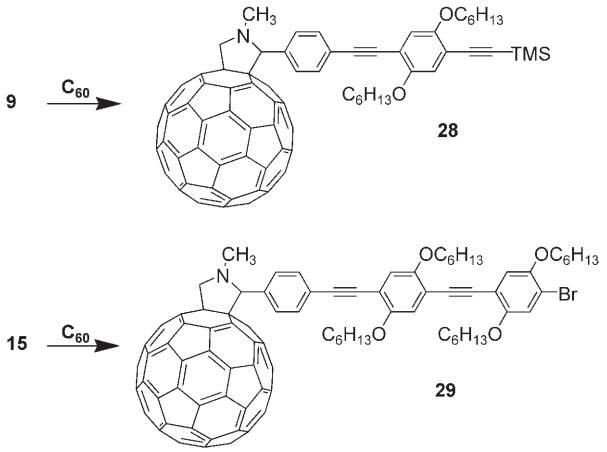

Scheme 6. General conditions for the preparation of references are as follows: *N*-methylglycine, Δ, 3 h in chlorobenzene.

The electronic absorption spectra of exTTF–oPPE–C_{60} reveal the presence of the typical bands of C_{60}, exTTF and oPPE. Figure 1 shows a comparison, as a representative example, of the UV-visible spectrum of exTTF–oPPE–C_{60} (**27b**) with exTTF–oPPE (**26b**) and **28**. A bathochromic shift was observed for **27b** relative to the corresponding reference compound (**28**). The increase of the π-conjugated system between the electroactive units in **27a–c** resulted in bathochromic shifts in the wavelength range from $\lambda = 431$ (monomer) to 494 nm (trimer) (see the Experimental Section in the Supporting Information).

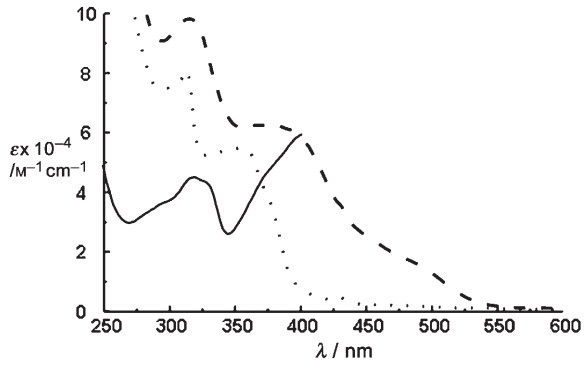

Figure 1. UV-visible spectrum of **27b** (– – –), **26b** (——) and **28** (·····).

It is interesting to note that **26b** shows a λ_{max} value at 460 nm that could be assigned to a charge-transfer band from the exTTF donor to the electron-accepting π-conjugat-

ed oligomer with a formyl group.[29] This band is bathochromically shifted in **27b** with the onset extending to nearly 600 nm.

Electrochemistry: The cyclic voltammetry (CV) data of exTTF–oPPE–C_{60} are collected in Table 3 along with those of C_{60}, exTTF and reference compounds **28** and **29**. The

Table 3. Redox potentials of **28**, **29**, **27a–c**, C_{60} and exTTF (V vs. SCE).[a]

Compound	E^1_{pa}	E^2_{pa}	E^3_{pa}	E^4_{pa}	E^1_{pc}	E^2_{pc}	E^3_{pc}	E^4_{pc}	E^5_{pc}
exTTF	0.33	–	–	–	–	–	–	–	–
C_{60}	–	–	–	–	−0.72	−1.12	−1.60		−2.05
28	–	–	1.16	1.47	−0.82	−1.23	−1.71	−1.76	–
29	–	–	1.14	1.44	−0.82	−1.21	−1.68	−1.74	–
27a	0.29	–	–	–	−0.82	−1.20	−1.69	−1.77	−2.03
27b	0.31	0.70	–	1.44	−0.82	−1.21	−1.62	−1.75	–
27c	0.35	0.68	0.92	–	–	−1.15	−1.60	−1.78	−1.94

[a] Pa: anodic peak; pc: cathodic peak. Glassy carbon working electrode, Ag/Ag^+ as reference electrode and platinum wire as counter electrode. Bu_4NClO_4 (0.1 M) as supporting electrolyte in *o*-dichlorobenzene/acetonitrile (4:1 v/v) as solvent. Scan rate: 200 mV s^{-1}.

measurements were carried out in ODCB/CH_3CN 4:1 (ODCB: *o*-dichlorobenzene) at room temperature using a glassy carbon (GC) working electrode, standard Ag/AgCl as the reference electrode and tetrabutylammonium hexafluorophosphate (0.1 M) as the supporting electrolyte (Table 3).

Unlike the parent C_{60}, the CV analysis of **28** and **29** showed four quasi-reversible reduction waves due to the fullerene moiety. These values are shifted towards more negative reduction potentials relative to pristine C_{60} due to the saturation of a double bond in the fullerene skeleton. Implicit is a raise of the LUMO energy of the resulting fullerene derivatives.[30] Compounds **28** and **29** also showed two oxidation waves (i.e., at 1.16 and 1.45 V) that correspond to the oligomer units.

The CV analysis of **27a–c** revealed the presence of four quasi-reversible reduction waves, resembling the trend found for the parent C_{60}. These reduction potentials are cathodically shifted relative to pristine C_{60} and appear at potential values similar to those found for the reference compounds. Furthermore, compounds **27a–c** exhibited one additional reduction potential wave due to the presence of the oligomer unit at −1.77 V (Figure 2).

The presence of exTTF leads only to one quasi-reversible oxidation wave involving a two-electron process to form the dication at around 0.33 V. This feature was previously confirmed by Coulometric analysis[31] and other related studies.[32] Attempts to generate and characterise the exTTF radical cation electrochemically caused its disproportionation to the neutral and the dicationic form.[33] The oxidation potential values in **27a–c** are anodically shifted relative to the parent exTTF, which confirms the better donor character of the triads. However, the increase of the length on the oligomer chain produces a slight cathodic shift between 0.29 and 0.35 V. Two additional oxidation waves at 0.7 and 1.4 V

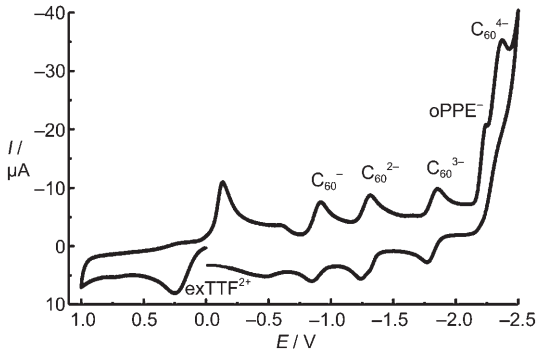

Figure 2. Cyclic voltammogram of **27a** (——) (see Table 3 for the experimental conditions).

were also observed due to the oxidation of the oligo(phenyleneethynylene) moiety.

Overall, the redox potentials of exTTF–oPPE–C_{60} (**27a–c**) are similar to those found for the pristine donor (exTTF) and acceptor (C_{60}). From this data and the absorption spectra, we conclude that there are only weak electronic interactions between the redox-active components in their ground states.

Theoretical calculations

Molecular geometries: Results from previous quantum chemical investigations led to the assumption that in the trimer exTTF–oPPE–C_{60} significant deviation from planarity prevails. In turn, we concluded that the lack of planarity in the dihedral angles between the phenyl rings adjacent to the pyrrolidine ring and to exTTF influences changes the π conjugation, and thus, the electronic coupling between donor and acceptor units in **27c**.[15] Further insight, by scrutinising higher levels of theory, indicates, nevertheless, that the inaccurate description of conjugated π systems, delocalised systems and rotation barriers as part of the previously used semiempirical Hamiltonians PM3 and AM1 might lead to a deviation from planarity.[34] Furthermore, the previously used geometry optimisation algorithm, as implemented in the HyperChem software package, was found to fail in achieving complete convergence. To validate the above-mentioned results we employed further calculations using the program packages Gaussian 03[35] for DFT and VAMP 10.0[36] for semiempirical calculations using the improved AM1* Hamiltonian. Semiempirical calculations suggested that in the minimum-energy structure the dihedral angle formed by the phenyl rings approaches zero. These results were confirmed by using DFT calculations at the B3LYP/6-31G* level and crosschecked by using B3PW91/6-31G* calculations. The deviation from planarity is less than ±12°. Furthermore, single-point calculations at the B3LYP/6-311G** and the B3PW91/6-311G** levels reveal a very low rotation barrier of the phenyl rings in the π-conjugated bridge (<2.0 kcal mol^{-1}). Rotations of the phenyl unit adjacent to the pyrrolidine and the benzene moiety of exTTF

connected to the oligomer are similarly not restricted by the relatively low rotation barrier of less than 1.0 kcal mol^{-1}.[34e]

Electronic structure and energy levels: Figure 3 shows the calculated (AM1*) ionization potentials (IPs) and electron affinities (EAs) of exTTF, C_{60}–pyrrolidine, the pristine

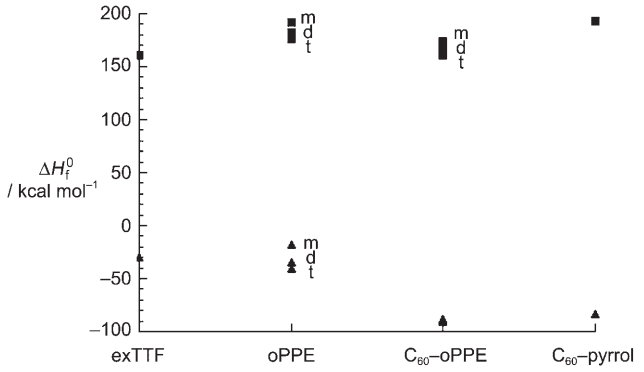

Figure 3. Calculated AM1* ionization potentials IP (▲) and electron affinities EA (■) of the pristine building blocks: monomers (m), dimers (d) and trimers (t).

oPPE oligomers and C_{60}–oPPE. exTTF exhibits the lowest EA and an IP that matches the IPs of the oligomer building blocks. With the addition of C_{60} to the oligomers the IP drops to approximately the IP of C_{60}–pyrrolidine, which suggests strong electronic coupling between C_{60} and the bridge. On the other hand, the electron-accepting features of the fullerene are represented by its highest EA, which confirms the electron-transfer pathway of the systems.

The HOMO/LUMO orbital schemes of the triads (Figure 4) manifest this donor–acceptor character. The HOMO is strongly localised on exTTF and reaches into the oPPE bridge, which facilitates electron injection into the bridge. However, in contrast to exTTF–oPPV–C_{60}, in which

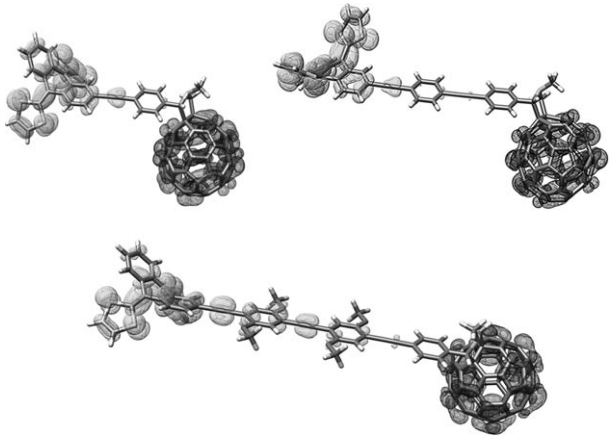

Figure 4. Representation of the HOMO (light grey) and LUMO (dark grey) orbitals of exTTF–oPPE–C_{60} as calculated at the B3LYP/6-31G* DFT level.

the HOMO is completely conjugated throughout the whole bridge, in the corresponding exTTF–oPPE–C_{60} the localization is more pronounced. Hence, injection of an electron into the bridge in exTTF–oPPV–C_{60} is favoured by the better orbital overlap between exTTF and the oligomers.

Local-electron-affinity[3537] mappings of exTTF–oPPE–C_{60} and exTTF–oPPV–C_{60} are represented in Figure 5. Signifi-

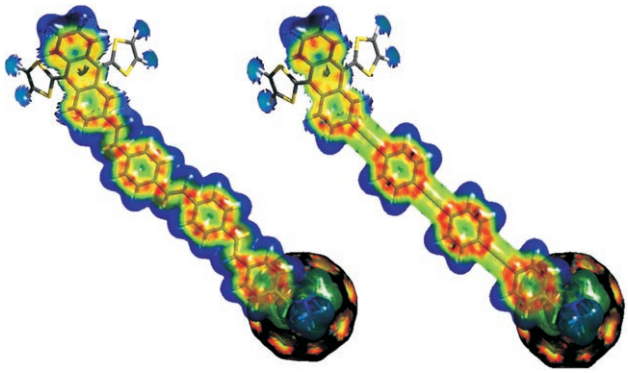

Figure 5. Local-electron-affinity maps of exTTF–oPPV–C_{60} (left) and exTTF–oPPE–C_{60} (right) as viewed with Tramp 1.1d[38].

cant differences between the two systems can be seen when comparing the conjugation in the bridge. In exTTF–oPPV–C_{60}, the local electron affinity is homogenously distributed throughout the whole bridge, whereas in the oPPE systems local maxima (red) can be found on the phenyl rings and minima (yellow) on the triple bonds. This is due to the polarising character of the triple bonds and their shorter bond lengths relative to the double bonds. Thus, the electron-transfer pathway through the oPPE bridge is interrupted by these ethynylene linkers. This strongly influences the charge-separation process and explains the difference in electron-transfer properties between exTTF–oPPE–C_{60} and exTTF–oPPV–C_{60}.

In summary, the electronic structure of all triads confirms the donor–bridge–acceptor character of the exTTF–oPPE–C_{60} systems and suggests that the HOMO→LUMO transition would represent a nearly complete charge-transfer excitation with a very low extinction coefficient. To gain better insight into these processes we carried out further calculations of the excited-state properties.

Quantum chemical modelling of excited states: To elucidate the geometrical relaxation processes postulated on the basis of the existence of very short-lived components in the time-resolved spectroscopic techniques described below, we optimised the minimum-energy geometries of the excited-states in a vacuum. These singles-only configuration (CIS) calculations predict that the HOMO→LUMO transition makes a major contribution to the charge-transfer (CT) state and causes a large change in dipole moment (Table 4).

One-electron excitation from the HOMO to the LUMO contributes to the CT state with zero oscillator strength (*f*)

Table 4. Excited-state properties predicted by quantum chemical calculations for compound **27c** (top: CIS including six active orbitals; bottom: CIS including ten active orbitals).

State	λ_{ex} [nm]	f	$\Delta\mu$ [D]	Character	Involved configuration
			CIS = 6		
S1	395	0.000	135.3	CT	HOMO→LUMO
S2	385	0.000	136.9	CT	HOMO→LUMO+1
			CIS = 10		
S2	376	0.066	3.6	LE1	HOMO−4→LUMO
S6	285	0.554	4.0	LE2	HOMO−4→LUMO+3
S7	278	0.000	129.3	CT	HOMO→LUMO, HOMO−2→LUMO
S8	277	0.001	69.8	BCT	HOMO−2→LUMO, HOMO−3→LUMO

(Table 4). In addition, in **27c** two symmetric bridge charge-transfer states (BCT) could be found close in energy to the CT states with a lower change in dipole moment (69.8 debye). These states correspond to the local-electron-affinity maxima centred on the oPPE rings, which underline the utility of the local electron affinity at the surface as a fast scanning method to elucidate possible CT states. These bridge CT states can compete with the charge transfer from exTTF to C_{60}. The calculated excitation wavelengths (in solution) for the CT states of the triads are found around $\lambda =$ 350 nm with a redshift that is dependent on the length of the oligomer but independent of solvent polarity. Similar behaviour was found for the fluorescence maxima of **27a–c** with a solvent-independent fluorescence, which reaches a maximum between $\lambda = 450$ and 500 nm and also depends on the length of the oligomeric bridge. However, regarding the fluorescence maximum of the BCT state of **27c** at 380 nm with a 261 nm excitation in simulated diethyl ether, an overlap between the CT fluorescence that reaches a maximum at 450 nm is possible and depends on the quantum yield.

Scrutinising the electrostatic potential of the AM1-optimised ground states and the corresponding CT states mapped onto the molecular surface (Figure S1 in the Supporting Information) reveals that in all CT states of the exTTF–oPPE–C_{60} triads the positive charge is localised on exTTF (red) and the negative charge on C_{60} (blue). Alternatively, in the BCT state the charge is localised on one of the phenyl rings. The corresponding symmetric BCT state was also found in the CI calculations. Further examination of the excited states reveals a strong dependence of their energy upon solvent polarity that follows the experimental trends (see Supporting Information).

Photophysics: First, the steady-state fluorescence spectra of the oPPE references C_{60}–oPPE and exTTF–oPPE–C_{60} were recorded upon 355 nm photoexcitation. For our photophysical assays we added the properties previously determined for the 0-mer, that is, the electron donor–acceptor system in which the anthracenoid core of exTTF is directly linked to the carbon atom of the pyrrolidine skeleton. In general, all oPPE references fluoresce strongly throughout the visible region, which renders this feature extremely valuable to dissect excited-state interactions with C_{60} in C_{60}–oPPE and also in exTTF–oPPE–C_{60}. The major oPPE features include strong visible-light fluorescence with quantum yields close to unity (i.e., about 0.77). The fluorescence maxima, similar to the absorption maxima, depend on the length of the oligomer and reach from 400 to 490 nm in the case of the monomer and trimer, respectively.

Not surprisingly, when inspecting the oPPE fluorescence in C_{60}–oPPE under identical experimental conditions dramatic changes, which are as large as a $1500\times$ reduction in the fluorescence quantum yields, attest to an almost instantaneous deactivation of the quantitatively excited oPPE in C_{60}–oPPE. Nevertheless, it is important to note that the fluorescence pattern of the oPPE is still preserved, despite the presence of C_{60}. In the near-infrared region of the fluorescence spectrum the observed features resemble those known for the C_{60} reference. Notably, photoexcitation at 355 nm directs the light nearly quantitatively to the oPPE and not to C_{60}. A reasonable explanation implies transduction of singlet excited-state energy from the oPPE (2.60 eV) to C_{60} (1.76 eV). Independent confirmation for this hypothesis was obtained from excitation spectra, in which the fluorescence wavelength was kept constant at 715 nm and the excitation wavelength was systematically varied. An exceptionally good agreement with the ground-state absorption spectrum confirms that the C_{60} fluorescence evolves largely from singlet energy transfer and, to a minor extent, from direct excitation. Quantification of the energy-transfer reaction was possible through comparing the C_{60} fluorescence quantum yields in solutions of C_{60}–oPPE in toluene with that of the C_{60} reference as an internal reference under exactly the same experimental conditions. Overall, the quantum yield of C_{60} fluorescence amounts to 6.0×10^{-4}—identical to that of a C_{60} reference that lacks oPPE—ruling out any endothermic electron transfer ($-\Delta G_{CS} > -0.24$ eV) between C_{60} (E_{red}: (0.61 ± 0.02) V versus Ag/Ag^+) and oPPE (E_{ox}: 2.09 (monomer **27a**), 2.04 (dimer **27b**) and 1.96 V (trimer **27c**) versus Ag/Ag^+). In conclusion, on exciting the oPPEs, a rapid intramolecular transduction of energy funnels the excited-state energy to the fullerene core, generating ^{1}*C_{60} quantitatively. Excitation of C_{60}, on the other hand, leads directly to ^{1}*C_{60}.

In stark contrast to C_{60}–oPPE and the C_{60} reference, the fullerene fluorescence is appreciably quenched in exTTF–oPPE–C_{60} (i.e., as low as 0.55×10^{-4} in THF). This is shown in Figure 6. Moreover, the fluorescence quantum yields depend strongly on the length of the oPPE bridge: 0-mer: 0.18×10^{-4}; monomer **27a**: 0.55×10^{-4}; dimer **27b**: 1.8×10^{-4}. No appreciable interactions were noted for the 3-mer. Setting these quantum yields in relationship to the C_{60} reference and its lifetime, the C_{60} fluorescence deactivation rates in the 0-mer, monomer **27a** and dimer **27b** were determined as 2.1×10^{10}, 6.6×10^{9} and 1.3×10^{9} s^{-1}, respectively. Additionally, we followed the fluorescence at 710 nm, but found only measurable decay rates for the C_{60} reference (6.6×10^{8} s^{-1}) and the dimer **27b** (2.6×10^{9} s^{-1}). We must conclude at this point of the investigation that ^{1}*C_{60}, populated either direct-

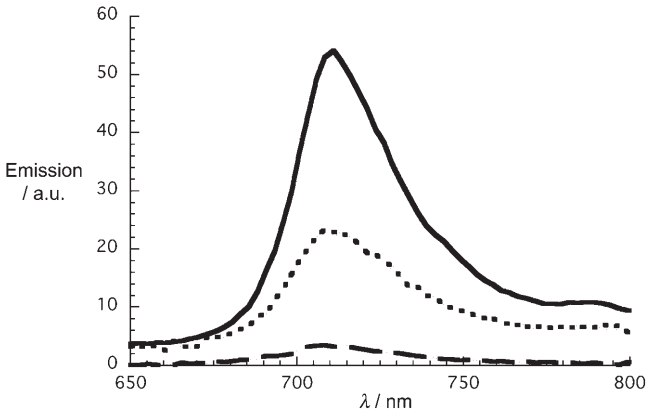

Figure 6. Quenching of the C_{60} emission in exTTF–oPPE–C_{60} (**27a**, **27b**) upon excitation at 425 nm with matching optical density at 425 nm in THF. ——=C_{60} reference, ·····=exTTF–oPPE$_2$–C_{60}, – – –=exTTF–oPPE$_1$–C_{60}.

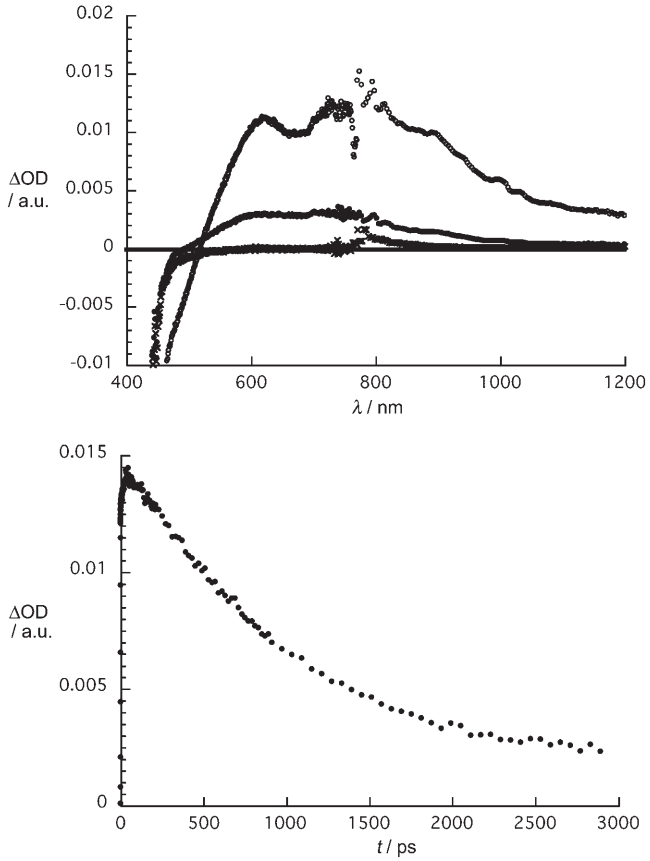

Figure 7. Top: differential absorption spectrum (visible and near-infrared) obtained upon femtosecond flash photolysis (420 nm) of solutions of reference trimer oPPE **16** in nitrogen-saturated THF with time delays between 0 and 3000 ps at room temperature (×=0, ●=1, and ○=2900 ps). Bottom: time-absorption profile of the spectra shown above at 800 nm to monitor the formation and decay of the singlet excited state of trimer oPPE.

ly or indirectly, powers an exothermic electron transfer ($-\Delta G_{CS} \approx 0.7$ eV) to yield the radical-ion-pair state, [exTTF$^{\bullet+}$–oPPE–$C_{60}^{\bullet-}$].

The aforementioned hypothesis, namely, formation of the radical-ion-pair state was corroborated through transient absorption spectroscopy. For oPPE, these results revealed the nearly instantaneous generation of metastable singlet excited-state transients upon photoexcitation. The spectral characteristics of these transients are ground-state bleaching in the 400–450 nm range and new transient absorption in the 600–1200 nm range (Figure 7). The product of the aforementioned decay is the corresponding triplet excited state of oPPE.

Upon photoexciting, C_{60}–oPPE transient species initially evolve that disclose features commonly seen in the oPPE references, namely, transient bleach (i.e., below 450 nm) and transient maxima (i.e., around 700 nm). Such an observation is important because it attests—in close agreement with the ground-state absorption at the 387 nm excitation wavelength—the successful excitation of the oPPE moieties. However, the features of the oPPE singlet excited state decay much faster than those observed for the intersystem-crossing (ISC) process in the oPPE references (Figure 8). Typical rate constants for this decay are of the order of $\approx 10^{12}\,s^{-1}$. Such values confirm the quantitative quenching of the oPPE fluorescence in C_{60}–oPPE. At the conclusion of the oPPE decay only the C_{60} singlet excited-state features are discernable, that is, a transient maximum at 880 nm. On a timescale of up to 3.0 ns the C_{60} singlet excited-state intersystem crosses to the corresponding triplet manifold. Importantly, the kinetics of the singlet decay and the triplet growth match each other reasonably well to yield ISC rates in C_{60}–oPPE of $6.5\times10^8\,s^{-1}$. The most prominent feature of the C_{60} triplet excited state is a 700 nm maximum as it evolves towards the end of the timescale of our femtosecond experiments (i.e., 3.0 ns). In complementary nanosecond experiments with C_{60}–oPPE the same triplet transient is seen, which in the absence of molecular oxygen, decays with multiexponential kinetics.

The additional detection from results of exTTF–oPPE–C_{60} of the instantaneous grow-in of the 880 nm absorption affirms the successful C_{60} excitation. Instead of seeing, however, the slow ISC dynamics that C_{60}–oPPE and C_{60} exhibit, the singlet–singlet absorption decays in the presence of exTTF donors with accelerated dynamics. The singlet excited-state lifetimes, as they were determined from an average of first-order fits of the time-absorption profiles at various wavelengths (850–950 nm), are listed in Table 5.

Spectroscopically, the transient absorption changes, taken after the completion of the decay, bear no resemblance to the C_{60} triplet excited state. Importantly, Figure 9 corroborates the spectral signatures of the one-electron oxidised exTTF$^{\bullet+}$ and the one-electron reduced $C_{60}^{\bullet-}$, which were detected as new transient maxima at 660 and 1010 nm, respectively. The spectral identification holds for the 0-mer, 1-mer and 2-mer, although for the 3-mer only a very broad transient, whose identity remains unknown to us at this stage, dominates the region of interest. It is, however, clear that no

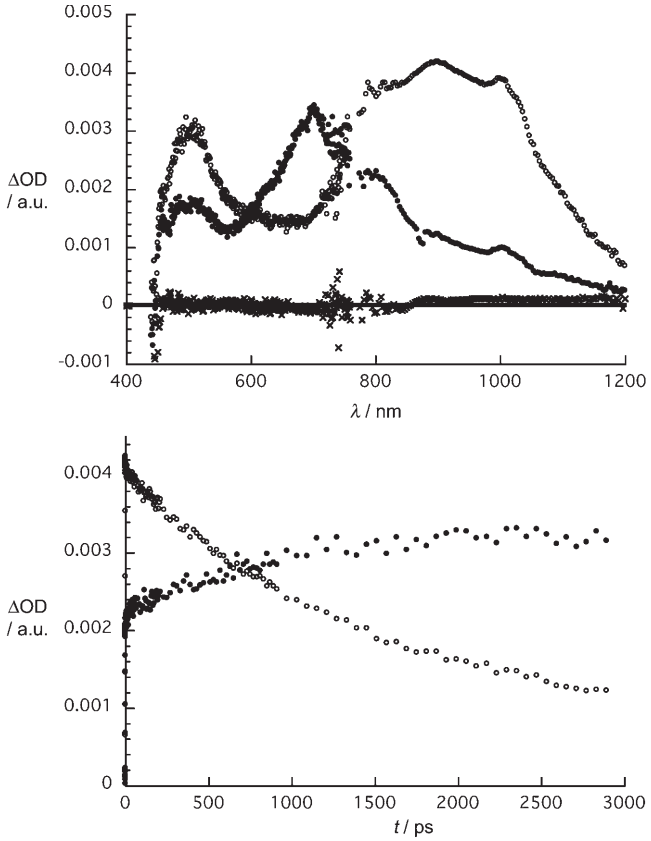

Figure 8. Top: differential absorption spectrum (visible and near-infrared) obtained upon femtosecond flash photolysis (420 nm) of solutions of reference C_{60}–oPPE **28** in nitrogen-saturated THF with time delays between 0 and 3000 ps at room temperature (×=0, ●=1, and ○=2900 ps). Bottom: time-absorption profile of the spectra shown above at 690 (●) and 900 nm (○) to monitor the formation and decay of the singlet excited state of C_{60}.

Table 5. Photophysical properties of the exTTF–oPPE–C_{60} triads and the fulleropyrrolidine.

	Φ_{fl}	τ_1[a] [ns]	k_{CS} [s^{-1}]	k_{CR} [s^{-1}]
C_{60} reference	6.0×10^{-4}	1.233	–	–
0-mer	0.18×10^{-4}	–	2.1×10^{10}	4.9×10^{6}
monomer **27a**	0.55×10^{-4}	–	6.6×10^{9}	1.1×10^{6}
dimer **27b**	1.8×10^{-4}	0.380	1.3×10^{9}	3.8×10^{5}
trimer **27c**	–	(0.793)	3.9×10^{8}	not detectable

[a] Singlet lifetime.

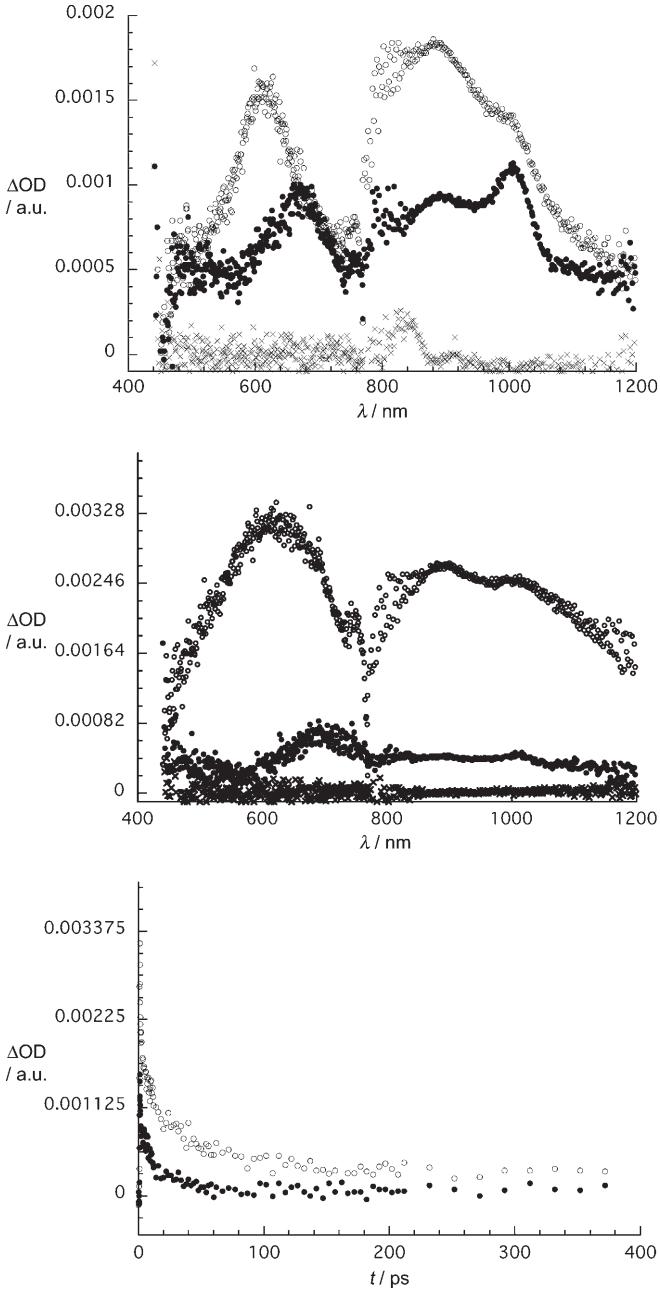

Figure 9. Top: differential absorption spectrum (visible and near-infrared) obtained upon femtosecond flash photolysis (477 nm) of solutions of monomer **27a** in nitrogen-saturated THF with time delays between 0 and 3000 ps at room temperature (×=0, ●=1, and ○=2900 ps). Middle: differential absorption spectrum (visible and near-infrared) obtained upon femtosecond flash photolysis (477 nm) of solutions of dimer **27b** in nitrogen-saturated THF with several time delays between 0 and 3000 ps at room temperature (×=0, ●=1, and ○=2900 ps). Bottom: time-absorption profile of the spectra shown above at 1010 nm to monitor the formation of the radical-ion-pair state (●=monomer **27a**, ○=dimer **27b**).

radical ion pair is formed for the 3-mer (see below). Both radical-ion-pair species, that is, $C_{60}^{\bullet-}$ and $exTTF^{\bullet+}$, decay in the 0-mer ($4.9\times10^{6}\,s^{-1}$), monomer **27a** ($1.1\times10^{6}\,s^{-1}$) and dimer **27b** ($3.8\times10^{5}\,s^{-1}$) with similar rates ($-\Delta G_{CR}\approx1.0$ eV) to reinstate the singlet ground states.

Figure 10 documents how relating the charge-separation and charge-recombination dynamics in THF to the electron donor–acceptor separation (i.e., centre-to-centre: R_{CC}) allows the evaluation of the attenuation factor (β) of the oPPE bridges. From both relationships, which reveal linear dependences, attenuation factors (β) were derived that are in perfect agreement with each other. In particular, (0.21 ± 0.05) $Å^{-1}$ was determined for the charge separation, whereas (0.2 ± 0.05) $Å^{-1}$ evolved for the charge recombination. Please note that these values are factors of 20 and 2 higher

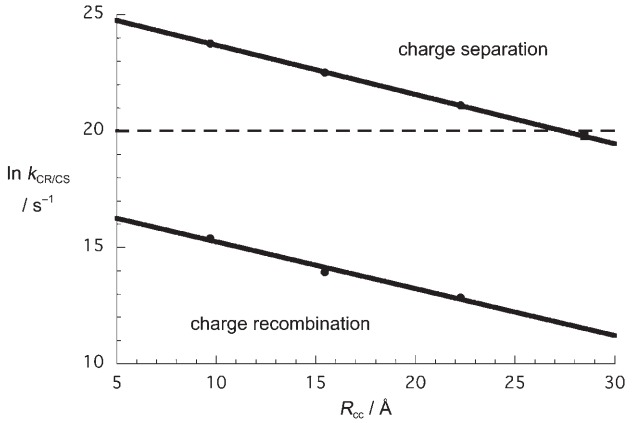

Figure 10. Centre-to-centre distances (R_{CC}) dependence of charge-separation ($\ln k_{CS}$) and charge-recombination ($\ln k_{CR}$) rate constants in exTTF–oPPE–C_{60} in nitrogen-saturated THF at room temperature. The slope represents β. The dashed line represents the singlet lifetime of C_{60}.

than what we have established earlier for oPPV bridges (i.e., (0.01 ± 0.005) Å^{-1})[13,14] and oligofluorene [oFl] bridges (i.e., (0.09 ± 0.005) Å^{-1}),[39] respectively.

It is interesting to note that by extrapolating the linear relationship in Figure 10 to the trimer **27c** a charge-separation rate would be obtained that would, in fact, be slower than the singlet lifetime of C_{60} (i.e., dashed line). This, in turn, helps to rationalise the lack of C_{60} fluorescence quenching in the trimer **27c**.

Conclusion

We have successfully developed the synthesis of novel donor–bridge–acceptor (exTTF–oPPE–C_{60}) systems based on oligo(*p*-phenyleneethynylene) (oPPE) as a bridge. The combination of the bromo–iodo selectivity in the Hagihara–Sonogashira reaction and the selective deprotection of TMS-protected acetylene in the presence of a TIPS-protected acetylene is a powerful tool for the preparation of asymmetric oPPEs. A further cross-coupling reaction in a convergent manner leads to the respective dyads, endowed with an aldehyde group and an exTTF unit, which undergo a 1,3-dipolar cycloaddition reaction with C_{60} to afford the final molecular arrays **27a–c**.

The electrochemical study reveals amphoteric redox behaviour and a lack of significant electronic communication between the donor (exTTF) and the acceptor (C_{60}) moieties through the π-conjugated oligomer in the ground state. However, quantum chemical calculations disclose the donor–bridge–acceptor character of the exTTF–oPPE–C_{60} systems and suggest that the HOMO→LUMO transition would represent a nearly complete charge-transfer excitation with a very low extinction coefficient. Photoexcitation is followed by a rapid intramolecular charge separation to generate a radical-ion-pair state (exTTF and C_{60} at 660 and 1000 nm, respectively). The radical ion pairs decay in 4.9×10^6 (**27a**) and 1.1×10^6 s^{-1} (**27b**). The charge-recombination dynamics reveal a wirelike behaviour with an attenuation factor (β) of (0.2 ± 0.05) Å^{-1}.

Acknowledgements

This work was supported by the MEC of Spain (project CT2005-02609/BQU and Consolider-Ingenio 2010C-07-25200), the CAM (project P-PPQ-000225-0505), the Deutsche Forschungsgemeinschaft (SFB 583), FCI and the Office of Basic Energy Sciences of the U.S. Department of Energy.

[1] a) F. L. Carter, *Molecular Electronic Devices*, Dekker, New York, **1987**; b) J. Jortner, M. A. Ratner, *Molecular Electronics*, Blackwell, London, **1997**; c) *Photoinduced Electron Transfer* (Eds.: M. A. Fox, M. Chanon), Elsevier, Amsterdam, **1998**; d) R. L. Carrol, C. B. Gorman, *Angew. Chem.* **2002**, *114*, 4556; *Angew. Chem. Int. Ed.* **2002**, *41*, 4378; e) *Electron Transfer in Chemistry* (Ed.: V. Balzani), Wiley-VCH, Weinheim, **2001**; f) W. W. Parson, *Photosynth. Res.* **2003**, *76*, 81–92; g) The Special Issue on Organic Electronics: *Chem. Mater.* **2004**, *16*, 4381–4846; h) The Special Issue on Molecular Wires and Electronics: *Top. Curr. Chem.* **2005**, *257*, 1, 33–62.

[2] a) R. H. Goldsmith, L. E. Sinks, R. F. Kelley, L. J. Betzen, W. Liu, E. A. Weiss, M. A. Ratner, M. R. Wasielewski, *Proc. Natl. Acad. Sci. U.S.A.* **2005**, *102*, 3540–3545; b) E. A. Weiss, M. J. Tauber, R. F. Kelley, M. J. Ahrens, M. A. Ratner, M. R. Wasielewski, *J. Am. Chem. Soc.* **2005**, *127*, 11842–11850; c) M. J. Tauber, R. F. Kelley, J. M. Giaimo, B. Rybtchinski, M. R. Wasielewski, *J. Am. Chem. Soc.* **2006**, *128*, 1782–1783; d) R. H. Goldsmith, M. R. Wasielewski, M. A. Ratner, *J. Phys. Chem. A* **2006**, *110*, 20258–20262.

[3] a) K. Müllen, G. Wegner, *Electronic Materials: The Oligomer Approach*, Wiley-VCH, Weinheim, Germany, **1998**.

[4] a) J. F. Nierengarten, J. F. Eckert, J. F. Nicoud, L. Ovali, V. Krasnikov, G. Hadziioannou, *Chem. Commun.* **1999**, 617–618; b) D. M. Guldi, C. Luo, A. Swart, R. Gómez, J. L. Segura, N. Martín, C. Brabec, N. Saricifti, *J. Org. Chem.* **2002**, *67*, 1141–1152; c) J. L. Segura, N. Martín, D. M. Guldi, *Chem. Soc. Rev.* **2005**, *34*, 31–47; d) T. M. Figueira-Duarte, A. Gégout, J. F. Nierengarten, *Chem. Commun.* **2007**, 109–119.

[5] a) E. Peeters, P. A. van Hal, J. Knol, C. J. Brabec, N. S. Sariciftci, J. C. Hummelen, R. A. J. Janssen, *J. Phys. Chem. B* **2000**, *104*, 10174–10190; b) T. Gu, D. Tsamouras, C. Melzer, V. Krasnikov, J. P. Gisselbrecht, M. Gross, G. Hadziioannou, J. F. Nierengarten, *ChemPhysChem* **2002**, 124–127.

[6] a) K. G. Thomas, V. Biju, D. M. Guldi, P. V. Kamat, M. V. George, *J. Phys. Chem. B* **1999**, *103*, 8864–8869; b) D. M. Guldi, A. Swartz, Ch. Luo, R. Gomez, J. L. Segura, N. Martín, *J. Am. Chem. Soc.* **2002**, *124*, 10875–10886.

[7] a) N. P. Redmore, I. V. Rubstov, M. J. Therien, *J. Am. Chem. Soc.* **2003**, *125*, 8769; b) T. O. Screen, J. R. G. Thorne, R. G. Denning, D. G. Bucknall, H. L. Anderson, *J. Mater. Chem.* **2003**, *13*, 2796–2808.

[8] T.-Y. Dong, S.-W. Chang, S.-F. Kin, M.-C. Lin, Y.-S. Wen, L. Lee, *Organometallics* **2006**, *25*, 2018–2024.

[9] a) N. Martín, L. Sánchez, B. Illescas, I. Pérez, *Chem. Rev.* **1998**, *98*, 2527–2548; b) D. M. Guldi, N. Martín, *J. Mater. Chem.* **2002**, *12*, 1978–1992; c) *Fullerenes: From Synthesis to Optoelectronic Properties* (Eds.: D. M. Guldi, N. Martín), Kluwer Academic Publishers, Dordrecht, **2002**; d) F. Giacalone, N. Martín, *Chem. Rev.* **2006**, *106*, 5136–5190.

[10] W. B. Davis, W. A. Svec, M. A. Ratner, M. R. Wasielewski, *Nature* **1998**, *396*, 60–63.

[11] G. Pourtis, D. Beljonne, J. Cornil, M. A. Ratner, J. L. Brédas, *J. Am. Chem. Soc.* **2002**, *124*, 4436–4447.

[12] E. A. Weiss, M. J. Ahrens, L. W. Sinks, A. V. Gusev, M. A. Ratner, M. R. Wasielewski, *J. Am. Chem. Soc.* **2004**, *126*, 5577–5584.

[13] F. Giacalone, J. L. Segura, N. Martín, D. M. Guldi, *J. Am. Chem. Soc.* **2004**, *126*, 5340–5341.
[14] a) G. de la Torre, F. Giacalone, J. L. Segura, N. Martín, D. M. Guldi, *Chem. Eur. J.* **2005**, *11*, 1267–1280; b) F. Giacalone, J. L. Segura, N. Martín, D. M. Guldi, *Chem. Eur. J.* **2005**, *11*, 4819–4834.
[15] For a preliminary communication, see: C. Atienza, N. Martín, M. Wielopolski, N. Haworth, T. Clark, D. M. Guldi, *Chem. Commun.* **2006**, *30*, 3202–3204. See also: a) C. Wang, A. S. Batsanov, M. R. Bryce, I. Sage, *Org. Lett.* **2004**, *6*, 2181–2184; b) Y. Shirai, Y. Zhao, L. Cheng, J. M. Tour, *Org. Lett.* **2004**, *6*, 2129–2132; c) J.-F. Nierengarten, T. Gu, G. Hadziioannou, V. Lrasnikov, *Helv. Chim. Acta* **2004**, *87*, 2804–2805; d) W. Hu, H. Nakashima, K. Furukawa, Y. Kashimura, K. Ajito, Y. Liu, D. Zhu, K. Torimitsu, *J. Am. Chem. Soc.* **2005**, *127*, 2804–2805; e) C. Wang, L.-O. Palsson, A. S. Batsanov, M. R. Bryce, *J. Am. Chem. Soc.* **2006**, *128*, 3789–3799.
[16] a) K. Sonogashira in *Comprehensive Organic Synthesis* (Eds.: B. M. Trost, I. Fleming), Pergamon Press, Oxford, **1991**; b) K. Sonogashira in *Metal-Catalyzed Cross-Coupling Reactions* (Eds.: F. Diederich, P. J. Stang), Wiley-VCH, Weinheim, **1998**, 203; c) K. Sonogashira, *J. Organomet. Chem.* **2002**, *653*, 46–49; d) S. Eisler, N. Chahal, R. McDonald, R. R. Tykwinski, *Chem. Eur. J.* **2003**, *9*, 2542–2550; e) W. Mohr, J. Stahl, F. Hampel, J. A. Galysz, *Chem. Eur. J.* **2003**, *9*, 3324–3340; f) S. Eisler, A. D. Slepkov, E. Elliott, T. Luu, R. McDonald, F. A. Hegmann, R. R. Tykwinski, *J. Am. Chem. Soc.* **2005**, *127*, 2666–2676.
[17] a) K. Sonogashira, Y. Tohda, N. Hagihara, *Tetrahedron Lett.* **1975**, *16*, 4467–4470; b) Y. Tohda, K. Sonogashira, N. Hagihara, *Synthesis* **1977**, 777–778.
[18] a) R. Diercks, K. P. C. Vollhardt, *Angew. Chem.* **1986**, *98*, 268–270; *Angew. Chem. Int. Ed. Engl.* **1986**, *25*, 266–268; b) R. D. Bradshaw, L. Guo, C. A. Tessier, W. G. Youngs, *Organometallics* **1996**, *15*, 2582–2584.
[19] a) Q. Zhou, P. J. Carroll, T. M. Swager, *J. Org. Chem.* **1994**, *59*, 1294–1301; b) S. Höger, A.-D. Meckenstock, S. Müller, *Chem. Eur. J.* **1998**, *4*, 2423–2434; c) M. Mayor, C. Didschies *Angew. Chem.* **2003**, *115, 3284–3287; Angew. Chem. Int. Ed.* **2003**, 42, 3176–3179; *Angew. Chem. Int. Ed.* **2003**, *42*, 3176–3179; d) F. Maya, J. M. Tour, *Tetrahedron* **2004**, *60*, 81–92.
[20] a) H. Meier, D. Ickenroth, U. Stalmach, K. Koynov, A. Bathiar, C. Bubeck, *Eur. J. Org. Chem.* **2001**, *23*, 4431–4443; b) D. Ickenroth, S. Weissmann, N. Rumpf, H. Meier, *Eur. J. Org. Chem.* **2002**, *16*, 2808–2814.
[21] a) K. Sonogashira, *Comprehensive Organic Synthesis, Vol. 3*, Pergamon, Oxford, **1990**; b) Q. Zhou, P. J. Carroll, T. M. Swager, *J. Org. Chem.* **1994**, *59*, 1294–1301; c) *Modern Acetylene Chemistry* (Eds.: P. J. Stang, F. Diederich), VCH, Weinheim, **1995**; d) K. Sonogashira, *J. Organomet. Chem.* **2002**, *653*, 46–49.
[22] D. B. Wertz, R. Gleiter, F. Rominger, *J. Org. Chem.* **2004**, *69*, 2945–2952.
[23] M. Ravikanth, J.-P. Strachan, F. Li, J. S. Lindsey, *Tetrahedron* **1998**, *54*, 7721–7734.
[24] a) S. Kawabata, N. Tanabe, A. Osuka, *Chem. Lett.* **1994**, *101*, 1797–1800; b) A. Osuka, N. Tanabe, S. Kawabata, I. Yamazaki, Y. Nishimura, *J. Org. Chem.* **1995**, *60*, 7177–7185; c) D. A. M. Egbe, C. Ulbricht, T. Orgis, B. Carbonnier, T. Kietzke, M. Peip, M. Metzner, M. Gericke, E. Birckner, T. Pakula, D. Neher, U.-W. Grummt, *Chem. Mater.* **2005**, *17*, 6022–6032.
[25] F. W. Hartner, Y. Hsiao, K. K. Eng, N. R. Rivera, M. Palucki, L. Tan, N. Yasuda, D. L. Hughes, S. Weissman, D. Zewge, T. King, D. Tschaen, R. P. Volante, *J. Org. Chem.* **2004**, *69*, 8723–8730.
[26] D. V. Kosynkin, J. M. Tour, *Org. Lett.* **2001**, *3*, 993–995.
[27] a) R. W. Higgins, C. L. Hilton, S. D. Deochar, *J. Org. Chem.* **1951**, *16*, 1275–1277; b) H. O. House, D. G. Koepsell, W. J. Campbell, *J. Org. Chem.* **1972**, *37*, 1003–1011; c) M. C. Díaz, B. M. Illescas, C. Seoane, N. Martín, *J. Org. Chem.* **2004**, *69*, 4492–4499.
[28] a) M. Prato, M. Maggini, *Acc. Chem. Res.* **1998**, *31*, 519–526; b) N. Tagmatarchis, M. Prato, *Synlett* **2003**, 768–779.
[29] a) M. C. Diaz, M. A. Herranz, B. M. Illescas, N. Martín, N. Godbert, M. R. Bryce, C. Luo, A. Swartz, G. Anderson, D. M. Guldi, *J. Org. Chem.* **2003**, *68*, 7711–7721; b) B. Insuasty, C. Atienza, C. Seoane, N. Martín, J. Garin, J. Orduna, R. Alcala, B. Villacampa, *J. Org. Chem.* **2004**, *69*, 6986–6995.
[30] L. Echegoyen, L. E. Echegoyen, *Acc. Chem. Res.* **1998**, *31*, 593–601.
[31] a) M. R. Bryce, A. J. Moore, *J. Chem. Soc. Perkin Trans. 1* **1991**, 157–168; b) M. R. Bryce, A. J. Moore, *J. Chem. Soc. Chem. Commun.* **1991**, *22*, 1638–1639.
[32] a) A. S. Batsanov, M. R. Bryce, M. A. Coffin, A. Green, R. E. Hester, J. A. K. Howard, I. K. Lednev, N. Martín, A. J. Moore, J. N. Moore, E. Ortí, L. Sánchez, M. Savirón, P. M. Viruela, R. Viruela, T. Ye, *Chem. Eur. J.* **1998**, *4*, 2580; b) I. Pérez, S.-C. Liu, N. Martín, L. Echegoyen, *J. Org. Chem.* **2000**, *65*, 3796–3803; c) N. Martín, E. Ortí in *Handbook of Advanced Electronic and Photonic Materials and Devices, Vol. 3* (Ed.: H. S. Nalwa), Academic Press, New York, **2001**, Chapter 6.
[33] a) D. M. Guldi, L. Sanchéz, N. Martín, *J. Phys. Chem. B* **2001**, *105*, 7139–7144; b) A. E. Jones, C. A. Cristensen, D. F. Perepichka, A. S. Batsanov, A. Beeby, P. J. Low, M. R. Bryce, A. W. Parkle, *Chem. Eur. J.* **2001**, *7*, 973–978; c) C. Wang, L.-O. Palsson, A. S. Batsanov, M. R. Bryce, *J. Am. Chem. Soc.* **2006**, *128*, 3789–3799.
[34] a) J. P. Stewart in *Reviews in Computational Chemistry, Vol. 3* (Eds.: K. B. Lipkowitz, D. B. Boyd), VCH, New York, **1991**, p. 45–48; b) N. T. Anh, G. Frison, A. Solladie-Cavallo, M. Patrick, *Tetrahedron* **1998**, *54*, 12841–12849; c) P. Burk, K. Herodes, I. Koppel, *Int. J. Quantum Chem. Symp.* **1993**, *27*, 633; d) M. J. S. Dewar, K. M. Dieter, *J. Am. Chem. Soc.* **1986**, *108*, 8075; e) Rotations in the monomer, dimer and trimer do not seem influence the electronic structure and the coupling between donor and acceptor. The rotational barriers comply with these found in the exTTF–oPPV–C_{60} triads (0.34 kcal mol^{-1}).
[35] Gaussian 03 (Revision D.02), M. J. Frisch, G. W. Trucks, H. B. Schlegel, G. E. Scuseria, M. A. Robb, J. R. Cheeseman, J. A. Montgomery, Jr., T. Vreven, K. N. Kudin, J. C. Burant, J. M. Millam, S. S. Iyengar, J. Tomasi, V. Barone, B. Mennucci, M. Cossi, G. Scalmani, N. Rega, G. A. Petersson, H. Nakatsuji, M. Hada, M. Ehara, K. Toyota, R. Fukuda, J. Hasegawa, M. Ishida, T. Nakajima, Y. Honda, O. Kitao, H. Nakai, M. Klene, X. Li, J. E. Knox, H. P. Hratchian, J. B. Cross, V. Bakken, C. Adamo, J. Jaramillo, R. Gomperts, R. E. Stratmann, O. Yazyev, A. J. Austin, R. Cammi, C. Pomelli, J. W. Ochterski, P. Y. Ayala, K. Morokuma, G. A. Voth, P. Salvador, J. J. Dannenberg, V. G. Zakrzewski, S. Dapprich, A. D. Daniels, M. C. Strain, O. Farkas, D. K. Malick, A. D. Rabuck, K. Raghavachari, J. B. Foresman, J. V. Ortiz, Q. Cui, A. G. Baboul, S. Clifford, J. Cioslowski, B. B. Stefanov, G. Liu, A. Liashenko, P. Piskorz, I. Komaromi, R. L. Martin, D. J. Fox, T. Keith, M. A. Al-Laham, C. Y. Peng, A. Nanayakkara, M. Challacombe, P. M. W. Gill, B. Johnson, W. Chen, M. W. Wong, C. Gonzalez, J. A. Pople, Gaussian, Inc., Wallingford CT, **2004**.
[36] T. Clark, A. Alex, B. Beck, F. Burkhardt, J. Chandrasekhar, P. Gedeck, A. Horn, M. Hutter, B. Martin, G. Rauhut, W. Sauer, T. Schindler, T. Steinke, VAMP 10.0, Erlangen (Germany), **2003**.
[37] B. Ehresmann, B. Martin, A. H. C. Horn, T. Clark, *J. Mol. Model.* **2003**, *9*, 342–347.
[38] H. Lanig, R. Koenig, T. Clark, Tramp 1.1d, **2005**.
[39] C. Atienza-Castellanos, M. Wielopolski, D. M. Guldi, C. van der Por, M. R. Bryce, S. Filippone, N. Martín, *Chem. Commun.* **2007**, *48*, 5164–5166.

Received: January 25, 2008
Published online: June 13, 2008

